Environmental Science: Atmospheres

ROYAL SOCIETY OF CHEMISTRY

PAPER

Published on 09 July 2026

Cite this: DOI: 10.1039/d6ea00056h

Multi-method fingerprinting of airborne arsenic emissions from a copper smelter

Aaron J. Goodman, *[ab] Trystan Gagné,[a] Emmet Norris,[a] Houssame-Eddine Ahabchane,[a] Filip Kasprowicz,[c] Patrick L. Hayes [a] and Kevin J. Wilkinson *[a]

This study advances the characterization of airborne arsenic (As) emissions from a copper smelter. During two sampling campaigns, 155 aerosol samples were collected using two Coriolis-μ air samplers operated in parallel with high time resolution (every 8 minutes). Differences in As concentrations and As particle chemistries were determined at targeted locations, including inside the smelting reactor building and along the copper concentrate trucking route. These environments were sampled to determine the signature of As from the two most likely sources of emission: wind-blown copper concentrate from the smelter grounds and volatilized and recondensed As from the smelting process. Collection of the particles directly into Milli-Q water also enabled determination of the water-soluble As fraction by filtration. The chemistry and mineralogy of individual As-bearing particles were determined by single particle inductively coupled plasma time-of-flight mass spectrometry (spICP-ToF-MS), and scanning electron microscopy with energy dispersive spectroscopy (SEM-EDS). These single particle techniques validated our hypothesis regarding the use of the trace elements Sb, In and Bi in order to fingerprint particle origin. Using a combination of bulk and single particle fingerprinting strategies, we determined that the majority of the As measured off site was likely to have originated from the smelting process rather than from resuspended smelter inputs.

Received 26th April 2026
Accepted 30th June 2026

DOI: 10.1039/d6ea00056h

rsc.li/esatmospheres

Environmental significance

This study presents a comprehensive, high time resolution chemical analysis of arsenic-bearing aerosols emitted from a copper smelter. Previous studies of smelting emissions have been largely limited to total concentrations over 24–48 hours periods. Using Coriolis sampling devices to collect aerosol samples every 8 minutes, we demonstrate that the emissions are short transient phenomena, rendering current monitoring efforts ineffective. Furthermore, the chemistry of the aerosols with respect to solubility, and the multi-element chemistry of individual particles was used to fingerprint specific soures of arsenic from within the smelter site. The methods of air sampling and analysis in this study can be used to better understand point-source industrial emissions of metal aerosols worldwide.

1 Introduction

Arsenic (As) is a class 1 carcinogen causing deleterious impacts to humans.[1,2] Globally, as exposure is dominated by ingestion of contaminated food and drinking water, however in local environments, atmospheric exposure can also be a serious concern.[3–5] Non-ferrous metal smelting dominates global atmospheric emissions of As, with communities surrounding smelters at elevated risk for adverse health impacts.[6,7] Air monitoring around smelters often consists of the measurement of As concentrations with limited temporal resolution (*e.g.* 24–48 hours). Research into smelter emissions primarily involves passive sampling, although some previous studies collected particles directly from the plume *via* aircraft.[8–11] There are still significant knowledge gaps on the chemical speciation, mineralogy and sizes of the emitted As particles, all of which can impact toxicity.[12] Moreover, time-resolved As concentrations (short, high concentration emission events *vs.* consistent lower levels) are likely to provide information on specific operations responsible for emissions. Therefore, with respect to the smelting process, advances in the sampling and analysis of airborne As would be useful to increase our understanding of environmental risk and develop solutions to lower As emissions.

Sources of As emissions from smelters can be broadly grouped into two broad categories: dust mobilized from the transport, handling and storage of feedstock materials, and

[a]Department of Chemistry, Université de Montréal, Montréal, QC, Canada. E-mail: kj.wilkinson@umontreal.ca

[b]Department of Chemistry, Colorado School of Mines, Golden CO, USA. E-mail: agoodman@mines.edu

[c]Department of Geology and Geological Engineering, Colorado School of Mines, Golden CO, USA

direct emissions from the smelting process. The feedstock of the smelter studied herein is primarily copper concentrate, which contains some As-bearing sulfide minerals (*e.g.* enargite (Cu_3AsS_4) and tennantite ($Cu_6As_4S_{13}$)), and recycled copper streams (largely consisting of electronic waste).[13] At many smelters, including the one studied here, the concentrate is delivered by rail and truck, and it is transferred by machinery, often outdoors where fine particles can be mobilized by the wind. In the smelting process, the high temperature and oxygen fugacity in the reacting and converting steps facilitate the decomposition of As-bearing minerals and formation of gaseous As species (primarily As_2O_5).[14] Gases are collected and cleaned by electrostatic precipitators, but invariably some amount of gas escapes, generating fugitive emissions.[15] As the gases cool, solid phases condense which may include oxides, salts, native As, or solid solutions with other metals.[16]

This study provides key insights into As emissions from a copper smelter in Quebec by using several advanced methods of air sampling and analysis. Single particle inductively coupled plasma time-of-flight mass spectrometry (spICP-ToF-MS) provided multi-elemental fingerprints of the fine and ultrafine aerosols,[17] allowing for interpretation of As sources. Airborne As was sampled at a high frequency using Coriolis-μ air sampling devices; samples were collected every 8 minutes on multiple days. This study demonstrates several significant advances over our preliminary work at this site.[18] Previously, one Coriolis device was employed and only environments outside the boundaries of the smelter were sampled. Those results established the efficacy of the sampling and analytical approaches to characterize airborne metal(loid)s broadly, and allowed us to generate some hypotheses regarding their sources within the smelter. Namely, we hypothesized that specific combinations of trace elements within individual particles (Sn or In representing a contribution from recycled electronics, in combination with As, Sb, or Bi representing contribution from ore minerals) could be used as a marker of As-bearing aerosols that had condensed from vapor during the smelting process. By contrast, particles containing some combination of As, Sb, and/or Bi without In or Sn could be classified as originating from ore minerals, possibly sourced from wind-blown feedstock materials from the smelter grounds.

In this study, we were able to test these hypotheses through several advancements in sampling and analysis. First, we collected air samples at end-member environments inside smelter buildings and at strategic areas on the smelter property, in order to differentiate between the two hypothesized forms of airborne As emissions. Second, we employed two sampling devices to simultaneously measure different environments and different distances from the smelter. Third, the (operationally defined) water-soluble fraction of As was determined by immediately field filtering the captured particle suspensions. Fourth, our hypothesis regarding the particle chemistries was validated through scanning electron microscopy/energy dispersive spectroscopy (SEM-EDS) analysis of particles collected on filters. The insights gained from this study advance our understanding of the physicochemical nature of As-containing aerosols emitted from the smelter, helping to clarify their specific sources. Differentiating between these chemically distinct particle types is critical to inform emission control efforts at the site.

2 Methods and materials

2.1 Field sampling

Four sets of air samples were collected, each with 2 Coriolis samplers (Coriolis-μ device, Bertin Technologies) employed to capture different environments, or distances from the smelter. The first two sets were collected in April 2025, and the second two in June 2025 (Table 1). The first sample set was collected inside the reactor building, one sampler on the "load" side (Reactor Load, RL) where feedstock (copper concentrate, recycled materials) was loaded into the reactor, and one on the "vent" side, where the vents and gas exhaust systems were located (reactor vent, RV). The second sample set was collected outside the smelter buildings; one sampler was set up at the "truck tire wash", adjacent to the concentrate trucking route (truck wash, TW) with the other at the legal air monitoring station roughly 100 m outside the main gates of the smelter

Table 1 Sample set locations, numbers, and coordinates

Sample set	Date	Location	Abbreviation	Num. Samples	GPS coordinates
1	4/22/25	Reactor vent	RV	12	48.2538
		Reactor load	RL	12	−79.0154
2	4/23/25	Truck tire Wash	TW	18	48.2550
					−79.0118
		Legal station	LS	18	48.2499
					−79.0135
3	6/8/25	Ave Marcel Baril	AMB1	24	48.2602
					−79.0198
		Parc Dufresnoy	PD	24	48.2722
					−79.0208
4	6/10/25	Ave Marcel Baril	AMB2	24	48.2593
					−79.0099
		Chemin du Golf	CdG	24	48.2669
					−78.9980

(legal station, LS). The third and fourth sample sets were collected further off-site, at two fixed distances from the smelter, along downwind transects (listed in Table 1, mapped in Fig. 1). Wind roses are provided in Fig. S2.

The Coriolis sampling device vortexes air through a polycarbonate conical vessel that is filled with 15 mL of ultrapure water at an air flow rate of 300 L min^{-1}. Sample acquisition time was 6 minutes resulting in 1800 L of air being sampled. Cones were triple rinsed with ultrapure water between samples (2 minutes) so that consecutive samples were taken every 8 minutes. In order to account for evaporative losses that occurred as a result of the high flow rate, the vials of water were weighed in the field with a portable balance, before and after sample collection. After collection, samples were transferred to 15 mL HDPE metal-free tubes. For samples collected in April 2025 (RV, RL, TW, LS), two subsamples were generated: an unfiltered, unacidified sample for acid digestion and single particle analysis and a filtered, acidified sample for which the sample was first passed through a 25 mm nylon syringe filter (0.05 μm pore size, Tisch Scientific). The field collected filtrate was designed to give the water-soluble concentration of targeted airborne metal(loids). For sample sets collected in June, only one sub-sample was collected (unfiltered, unacidified). Field and laboratory blanks were collected and reported in Table S1. Laboratory blanks were collected by operating the Coriolis sampler in the laboratory, in an identical manner to how field samples were collected (running for 6 minutes at 300 L min^{-1}). Field blanks were collected at each sampling location immediately prior to the sampling period. 15 mL of ultrapure water was dispensed into the sampling cone, the cone was attached to the Coriolis sampler and allowed to sit for 6 minutes. The cone was then removed and the water was decanted into a 15 mL tube and split, with one fraction acidified for total metal(loid) concentrations, and the other unacidified for spICP-TOFMS. We note the possibility of contamination in one field blank (sample set TW) where concentrations in the blank were between 7–17%

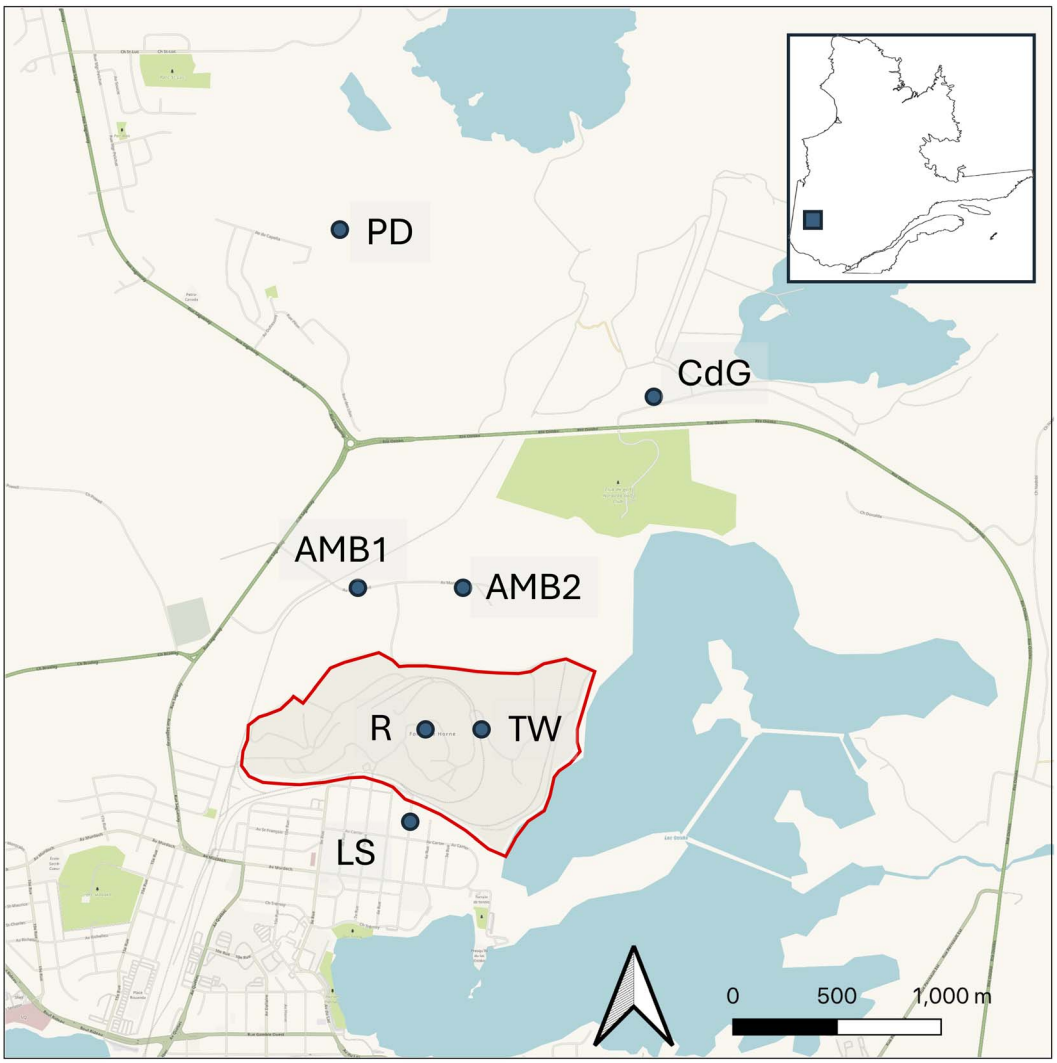

Fig. 1 Map of Rouyn Noranda, Quebec showing the outline of the smelter property in red and the locations of the sample sets. R = reactor (containing reactor load and reactor vent sub-sets), TW = truck wash, LS = legal station, MB1 = Ave Marcel Baril #1, MB2 = Ave Marcel Baril #2, PD = Parc Dufresnoy, CdG = Chemin du Golf.

of the average for the samples in this set. This suggests some contamination, but not to a level that impacts our interpretation. Contamination could arise from particles landing in the sampling cone or collection tube during sample transfer, either from the air or from the operator's hands (although gloves were worn).

One significant limitation of the Coriolis sampling device is the lack of data on the specific particle sizes collected. The collection efficiency is reported to be >90% for particles smaller than 10 μm, but this has not been verified for the very small, submicron particles considered in this study. Other particle-in-liquid sampling devices report lower efficiencies for small particles (as small as 300 nm), but these studies employed long collection times (*e.g.* 30–60 min) and suggested that small particles re-aerosolize from the collection cone.[19,20] In this study we used 6 minutes collection times, likely mitigating this issue. The particles measured in both this study and our previous work by spICP-ToF-MS are nearly all estimated to be <1 μm in diameter (see subsequent discussion). More than 7500 As-bearing particles in this size range were analyzed in this study, supporting the approach for source apportionment of sub-micron particles, regardless of the size-specific collection efficiency. If, on the other hand, there was a systematic difference in particle sizes between the two hypothesized As sources, our source apportionment would only be valid for the specific size range captured by the Coriolis sampler, and may differ from bulk PM results. Ongoing projects are employing filter-based air samplers with variable particle size cutoffs, as well as PM monitors to extend the source apportionment approach to bulk aerosols.

SEM-EDS data were acquired for 2 samples; (a) an air filter sample (MCV high volume, quartz fiber) collected 0.5 km downwind from the smelter boundary in October 2024 and (b) a sample of on-site road dust collected from the operator's sample archive (origin and specific location were not disclosed). The different sampling periods for the Coriolis and solid sample collection prevents any direct link between the findings from the SEM-EDS and the other analyses; however qualitative comparisons can be made.

Data from nearby and complementary atmospheric monitoring were made available to our research team and incorporated into this study. Atmospheric SO_2 is monitored at several locations around the smelter using a Thermo 43*i* analyzer based on UV emission, with 4 minutes data acquisition. SO_2 concentrations determined at the legal station overlap with the Coriolis sample set that was collected there.

2.2 Analysis

The unfiltered, unacidified subsamples were split in the laboratory; 3 mL aliquots were placed in separate 15 mL HDPE tubes and evaporated to dryness at 80 °C, then digested using 0.5 mL concentrated trace-metal grade HNO_3 and 50 μL H_2O_2 at 80 °C for 4 hours using a DigiPREP system (SCP Science). Digestions were first diluted with ultrapure water to 10 mL for ICP-MS analysis then subsequently diluted, based on the measured concentration to ensure a linear response within the ICP-MS calibration range.

Digested and filtered acidified samples were analyzed for total elemental concentrations using a NexION 5000 triple quadrupole ICP-MS (PerkinElmer) equipped with a concentric nebulizer and a glass cyclonic spray chamber. Calibration standards of 0.5, 2, 20, and 50 μg L^{-1} were prepared from 10 mg L^{-1} stock solutions in 2% ultrapure nitric acid. Terbium was added as an internal standard at 1 μg L^{-1} to correct for instrumental drift. A reference solution of 0.2 μg L^{-1} Co, In, Ce, and Pb, and a trace element certified reference material (NIST 1640a) were analyzed routinely to monitor performance (recoveries were between 80–120%). Elemental concentrations determined by ICP-MS were corrected for dilution, evaporative losses in the sampling device, and the volume of air sampled to obtain airborne metal(loid) concentrations in ng m^{-3}. A full suite of 34 elements was determined and reported in the supplementary data and associated data repository, but the results of this study focus on arsenic.[21]

Unfiltered, unacidified subsamples were analyzed by single particle ICP-ToF-MS (Vitesse, Nu Instruments) to measure the composition of individual submicron particles. Mass-to-charge ratios between 23 and 240 were monitored, with a "blanked" region between 30 and 41 to protect the instrument from Ar^+ and air ions.[22] The dwell time was 240 μs and the data acquisition time was 3 minutes per sample (three 60 s replicates). A hydrogen–helium gas mixture was used in the instrument's reaction cell to minimize polyatomic interferences. Dissolved aqueous standards between 1 and 20 μg L^{-1} were analyzed to determine instrument sensitivity and ultra-uniform 100 nm Au spheres (Nanocomposix) were analyzed to determine the transport efficiency using the number-based approach.[23] Raw ToF data were processed using the IsotopeTrack software[24] in which the particle detection threshold was calculated based on a compound-Poisson distribution with a false positive rate of 1×10^{-5}.[25] The number of detected particles was corrected for the transport efficiency, dilution, sample uptake rate, evaporative loss and the volume of air sampled in order to determine particle number and mass concentrations.

There are several uncertainties in spICP-ToF-MS, most notably the lack of size information for the detected particles. The mass of each detected element is reported and a spherical equivalent diameter (SED) is estimated, based on assumptions of shape and density. In this study we refer to the particles as "sub-micron" based upon the summed mass of all elements detected, and a conservative density of 2.5 g cm^{-3}. Under those assumptions, the SED of nearly all particles (>99%) is estimated to be less than 1 μm (Fig. S1). This likely represents the combined effect of natural particle size distributions (wherein small particles are logarithmically more abundant) and the reduced transport efficiency into the ICP of larger particles.[26] Additionally, we note that low-mass elements (C, O, S) were not detected by spICP-ToF-MS; while these elements would increase the mass of the particles substantially (*e.g.* 2.5× for Cu as $CuSO_4$), the cubed root relationship between mass and size would result in a rather modest increase in diameter (36% increase in diameter for the $CuSO_4$ example). Another source of uncertainty is the aggregation state of the particles. Although ultrasonication was used to disaggregate particles prior to

analysis, it is possible that some aggregates were introduced into the instrument. However, our results indicate that for the particle types considered here, detected multi-element compositions likely reflected individual particles rather than aggregates. Finally, dissolution of water-soluble phases impacts single particle data; in this study filtration and bulk analysis was used to approximate As solubility as a more robust measure than relying on the baseline signal which is often used to represent dissolved elemental concentrations in spICP-MS analysis. In this case, the baseline signal should not be used to determine dissolved As because some As-bearing aerosols were likely to have dissolved between collection and analysis (1–3 days). While our spICP-ToF-MS results therefore only represent the detectable insoluble aerosols, this equally impacts all sample sets, and the resulting source apportionment analysis remains valid.

The hi-vol filter sample was coated with carbon tape and the on-site road dust sample was mounted in epoxy resin and polished with alcohol to prevent dissolution of the water-soluble phases. Data were acquired using a TESCAN MIRA3 field emission SEM with a Schottky type field emission source, a yttrium aluminum garnet backscatter detector and a Bruker energy dispersive spectrometer. An acceleration voltage of 15 keV, beam intensity of 5 (unitless) and a working distance of 10 mm were used for the analysis.

3 Results and discussion

The results presented herein represent samples collected at pseudo-end member environments, with the data used for As source apportionment. We note that these environments are not perfect end members; some atmospheric deposition of both hypothesized sources of aerosols likely occurred at all sampling locations.

3.1 Variability of airborne arsenic concentrations with environment, distance, and time

Boxplots of total As concentrations measured in each sample set are presented in Fig. 2. Airborne As concentrations varied by nearly 4 orders of magnitude, with the highest As concentrations measured inside the reactor building (RL, RV) and on the smelter grounds (TW), ranging from 100 to 7000 ng m^{-3} (Fig. 2 and Table S2). By contrast, concentrations in samples collected outside the smelter boundary were far lower, ranging from 2 to 200 ng m^{-3}. Boxes of the same color indicate simultaneous collection, and thus concentrations can be meaningfully compared. Arsenic concentrations were on average 2.5× greater at the location where feedstock was loaded into the reactor, as compared to where the gases were vented, although the two sides of the building are not completely separated. The largest difference between the environments was for the truck wash and the legal station. Despite between separated by a distance of only 500 m, As concentrations were 35× greater at the truck wash. This result was likely due to the mobilization of feedstock dust from the roads, which appeared to be localized to the smelter grounds and largely not transported off site (see subsequent discussion).

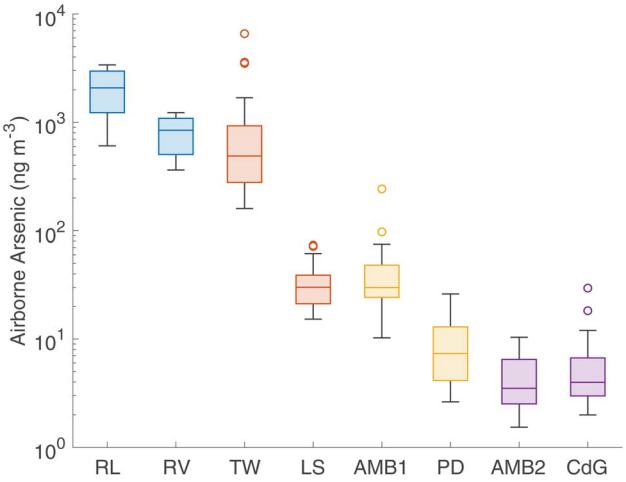

Fig. 2 Boxplots of total airborne arsenic concentrations measured for Coriolis-μ air samples collected inside and surrounding a copper smelter in Quebec, Canada. Boxes of the same color indicate the samples were collected simultaneously by two devices. RL = reactor load, RV = reactor vent, TW = truck tire wash, LS = legal station, AMB1 = Ave. Marcel Baril #1, PD = Parc Dufresnoy, AMB2 = Ave Marcel Baril 2, CdG = Chemin du Golf.

The sample sets of the two off-site locations of varying distance displayed different behaviors with respect to total As concentrations. In the first of these sample sets, As at site AMB1 (850 m from the smelter) was 5× that of PD (2.2 km from smelter) (Fig. 1). However, in the second set, site CdG (2.1 km from smelter) contained on average 1.5× more As than AMB2 (850m), despite both sites being downwind (Fig. S2). While total As measurements are critical to assess environmental impacts, additional information is needed to better attribute sources to the emissions. For example, many samples from the truck tire wash and the reactor vent sample sets overlapped in their As concentrations, however, as shown below, their sources were likely quite different.

Time-resolved As concentrations were highly variable in a variety of environments both within and surrounding the smelter complex. Major variations in airborne arsenic occurred on timescales as short as 10–20 minutes. At TW, AMB1, AMB2, PD and CdG, As varied by over 10× during the ∼3 hours sampling period, with As concentrations often spiking over 1–3 samples (*i.e.* peak of a duration of 8–24 minutes). At the truck wash (Fig. 3a), the spikes in total As at 15 : 15 and 16 : 15 reflect field observations; during these time periods, concentrate-hauling trucks drove within 5 m of the Coriolis sampler, suspending visible clouds of dust from the road, which persisted for several minutes before settling. This is also reflected by the overlapping PM_{10} spikes that were measured by PurpleAir sensors (Fig. S4). Each of the two distance-resolved sample sets (Fig. 3c and d) displayed a single transient spike in As concentration; however, in the first set, the spike was observed at the closer location (Fig. 3c), while in the second set it was observed at the more distant location (Fig. 3d). The spike observed in

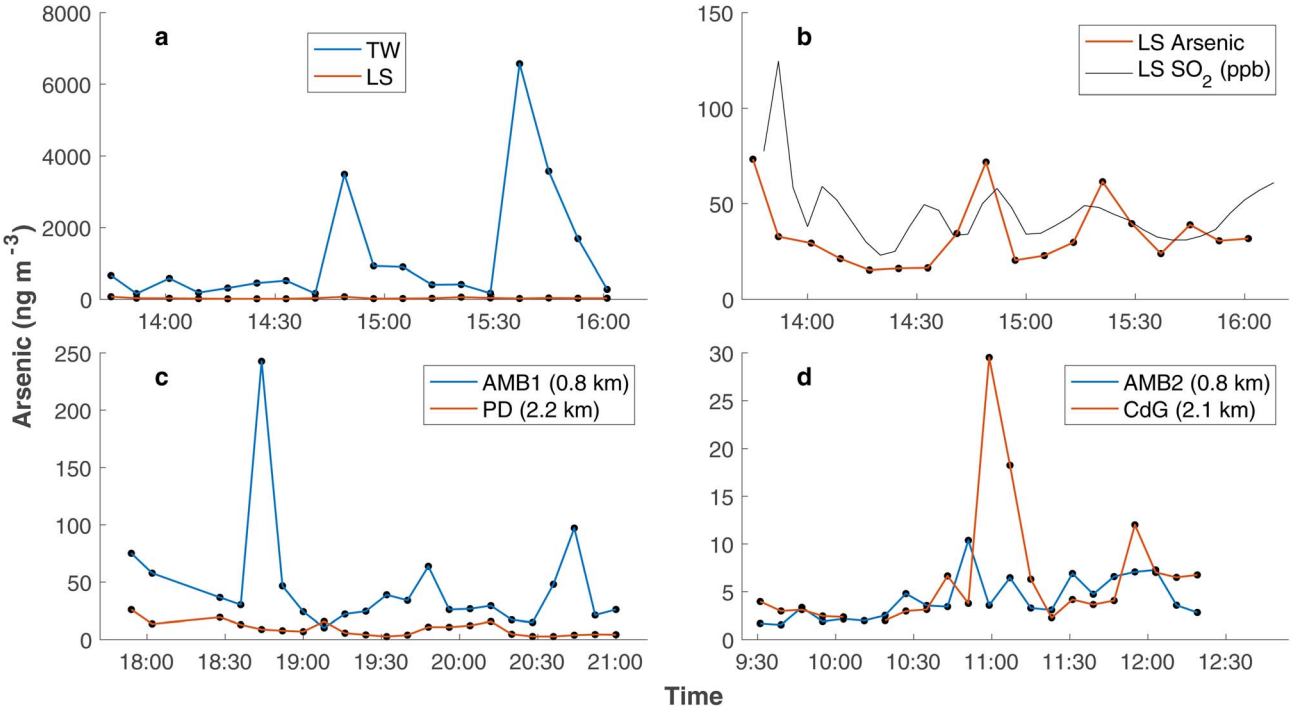

Fig. 3 Time-resolved concentrations of airborne arsenic for three paired sample sets; (a) truck wash and legal station, (c) Ave Marcel Baril #1 and Parc Dufresnoy, (d) Ave Marcel Baril #2 and Chemin du Golf. (b) legal station data were plotted separately with an expanded *y*-axis and overlaid with the airborne SO_2 concentrations that were measured at the station.

Fig. 3d was accompanied by a large visible emission from the smelter stack (Fig. S5) and the smell and taste of metal/sulfur at the CdG site. This may suggest that this specific spike in As could be attributed to the plume emanating from the smelter stack, thus tying it to the smelting process. We hypothesize that the AMB2 site was close enough to the stack that it was underneath the plume. The spike at AMB1 more likely originated from a ground-level fugitive emission, as the further downwind site did not show a spike, and there was no visible emission from the stack at 18 : 30. The As-bearing aerosols comprising this spike were likely diluted by ambient air, rendering As undetectable above the baseline concentration at the PD location. Confidence in these observations is increased based on the wind directions; during the sampling periods, the farther sites (PD, CdG) were located almost directly downwind of both the closer sites (AMB1 and AMB2), and the smelter itself (Fig. S2).

The sample set collected at LS, immediately outside the smelter boundary (Fig. 2b), showed some variability in airborne As over the sampling period (2.5 h), however, it was less than the other sets and without a significant short-term spike. Rather, As was elevated at the beginning of the time-series, falling to 20 ng m^{-3} during the first hour, before increasing again to 60–80 ng m^{-3} over the remaining 1.5 hours. This location was the only one where SO_2 measurements were available. SO_2 appeared to track the total As, with a peak at the start of the time-series and elevated but variable concentrations for the remainder. When SO_2 measurements were averaged to reflect the sampling period of the Coriolis measurements (6 min), a positive correlation, albeit weak, was observed ($r^2 = 0.37$, Fig. S3). Nonetheless, we note that due to the 2 minutes gap between successive Coriolis measurements, it was not possible to perfectly align the timing of two data sets.

The correspondence between the SO_2 and As emission trends may suggest that As was being emitted from the smelting process rather than from the mobilization of dust from the feedstock handling. PM concentrations, as measured by PurpleAir sensors, closely tracked the SO_2 and As trends with a short-term spike during the first 15 minutes (Fig. S4). The correspondence of PM_{10} with As concentrations at TW and LS suggests that both fugitive smelting emissions and dust from the feedstock handling contributed to the elevated PM; more work is needed to better understand the nature of the PM emission from the various sources.

3.2 Geochemical fingerprints of bulk arsenic

The two major sources of As (physically mobilized feedstock and material directly emitted from the smelting process) cannot be differentiated using only total As concentrations. Therefore, several indicators of As source were examined, using the pseudo-end member environments that were sampled for source apportionment. The first such indicator was the Cu : As ratio, which has been used previously to identify emissions from different steps in the smelting process.[27] The smelting process is designed to retain Cu and eliminate impurities, including As, which has a low volatilization temperature.[28] Thus, we hypothesized that the Cu : As ratio would be greater in the smelter feedstock than in the volatilized and re-condensed

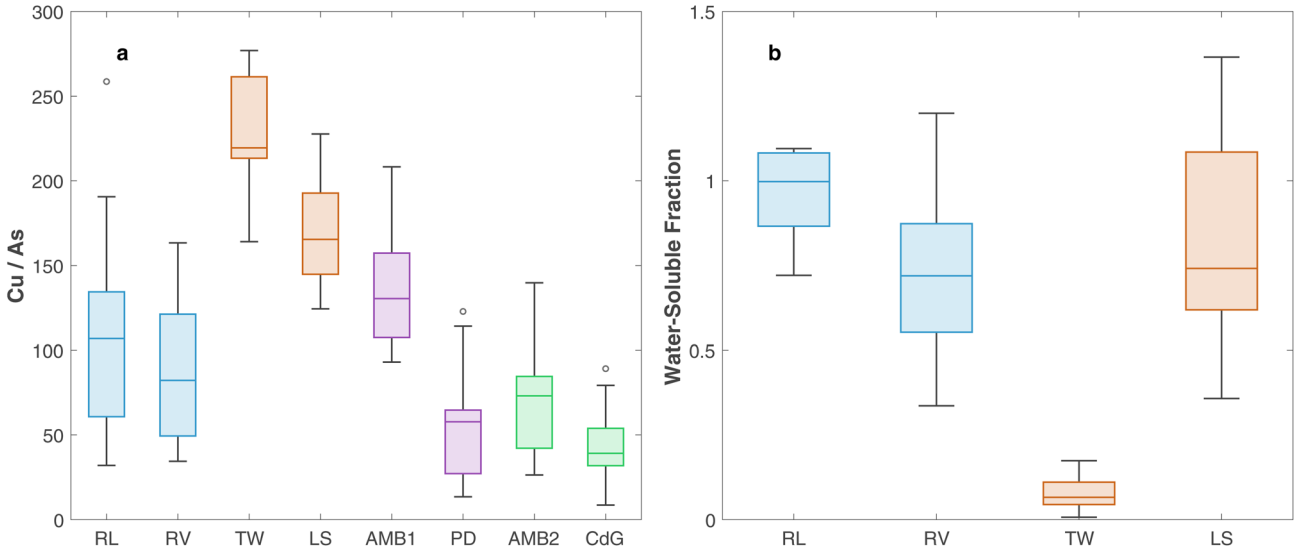

Fig. 4 (a) Copper : arsenic ratios measured across each sample set. (b) The water-soluble arsenic fraction in the four sample sets where it was measured. Water-soluble is operationally defined as the fraction in the 0.05 μm filtrate (samples were filtered in the field within 1 minute of collection in Milli-Q water).

material. Indeed, on average, a Cu : As ratio of 99 was measured at the reactor, which was 2.3× lower than what was measured at the truck wash (229) (Fig. 4a and Table S4). The average Cu : As ratio at the legal station was 171, intermediate between the truck wash and the reactor. If the truck wash and reactor samples represented perfect end-member emission sources of mobilized feedstock dust and high-temperature smelting vapors/condensates, respectively, then 55% of As measured at the legal station would be attributed to the former and 45% to the latter. Admittedly, there is uncertainty in this approach because these are not pure end members – some smelting emissions were likely captured in the air at the truck wash and some feedstock particles were likely captured inside the reactor building. Moreover, sample sets were collected on different days, possibly with differing feedstock composition.

The sample sets obtained farther from the smelter complex generally display lower Cu : As ratios, consistent with a hypothesis that fugitive smelting emissions could travel further than the wind-blown dust. Whether ground-level or from the stack, smelting emissions originate from a higher elevation as compared to the wind-blown feedstock particles, and are likely to occur in smaller size fractions.[29] In the distance-based sample sets, the site that was furthest from the smelter displayed the lowest Cu : As ratio, consistent with this hypothesis. Because the four sample sets were collected on different days, differences in smelting activities and/or feedstock composition (which are proprietary information) were likely to influence the precise Cu : As ratios that were measured and thus any source apportionment from this approach is subject to some uncertainty.

The solubility of the As containing aerosols may also provide an effective means to discriminate sources. For the sample sets inside the reactor (RL and RV), 40–100% of the As was attributed to the water-soluble fraction (Fig. 4b and Table S5). Indeed, several of these values were >100% (the filtered acidified concentration was greater than the total concentration). The most likely explanation for this observation was the additional deposition of As-bearing phases into the sample vial during filtration and sample transfer, as the filtration required the collection tubes to be open for longer compared to the unfiltered samples. Care was taken to avoid contamination, but we could not guarantee this given the high ambient arsenic concentrations in the reactor building. This impacted a minority of the samples, and although is non-ideal behavior, we take the values >100% to indicate that all or nearly all of the As was water-soluble. On the other hand, at the TW, very little As was water-soluble (0.7–26%, mean 8%). Similar to the values at the reactor, arsenic at LS was highly soluble, comprising between 40 and 100% (Table S5). The As in feedstock materials is likely contained within sulfide mineral particles; dissolution of these phases is kinetically limited for the short times imposed prior to filtration (~1 min following sample collection). In contrast, As phases emitted from the smelting process are likely to be freshly condensed oxides or salts. Nonetheless, to our knowledge, there have been no reports of this degree of As solubility from smelter emissions. While As solubilization from a smelting flue dust was reported to be highly variable (5–92% soluble in a TCLP solution),[30] experiments were performed at pH 2.8 with a leaching time of 18 hours. Clearly the majority of As measured at the reactor and at the legal station was soluble, even when using very short contact times (Fig. 4B). It is known that condensed aerosols from smelting off-gases evolve over time, eventually recrystallizing to more thermodynamically stable phases.[14] Thus, our approach of capturing particles directly into water rather than on filters and immediately filtering in the field provides new information on the nature of freshly condensed smelter-derived particles. On the other hand, the approach is limited by our inability to precisely control the

timing and the chemistry of the solution in which the particles dissolve; variable concentrations of SO_2 in air would yield variable pH of the collection water. In spite of this restriction, the results are highly useful for understanding As emissions from Cu smelting. Based upon the similar solubilities observed at LS and RV, As measured at the legal station could be interpreted as originating almost entirely from the smelting process.

3.3 Chemistry and mineralogy of individual particles: spICP-ToF-MS and SEM-EDS

While bulk geochemical signatures clearly indicated differences in the nature of the As emission sources from the smelter, even greater insights could be gained from the examination of individual particles. To that end, we employed spICP-ToF-MS to determine the composition of individual submicron As-bearing phases in four of the sample sets (reactor vent, reactor load, truck wash, legal station). In our previous study, we developed a fingerprinting strategy to discriminate emission sources based on the presence of specific groups of trace elements.[18] The feedstock of this Cu smelter is composed of ore minerals (some of which contain As, Bi, and Sb) and recycled Cu (largely electronics which likely contain In). Therefore, based upon the assumption that these elements would be combined during volatilization and condensation,[31] particles containing a combination of In and As/Sb/Bi are likely to originate from the smelting process. In contrast, particles from the recycling waste stream are unlikely to contain As/Sb/Bi, and ore concentrates rarely contain appreciable indium concentrations (except at ppm levels in some occurrences of chalcopyrite).[32,33] Thus, if a particle contains Cu along with some combination of As/Sb/Bi, but no In, it is more likely to be an ore mineral particle. Fig. 5 presents the ten most frequently observed As particle types with respect to these elements at the end member environments: TW (Fig. 5a and b) and RV. Full multi-element particle results are available in the associated data repository. The major difference in the multi-element signature of As particles is the presence of

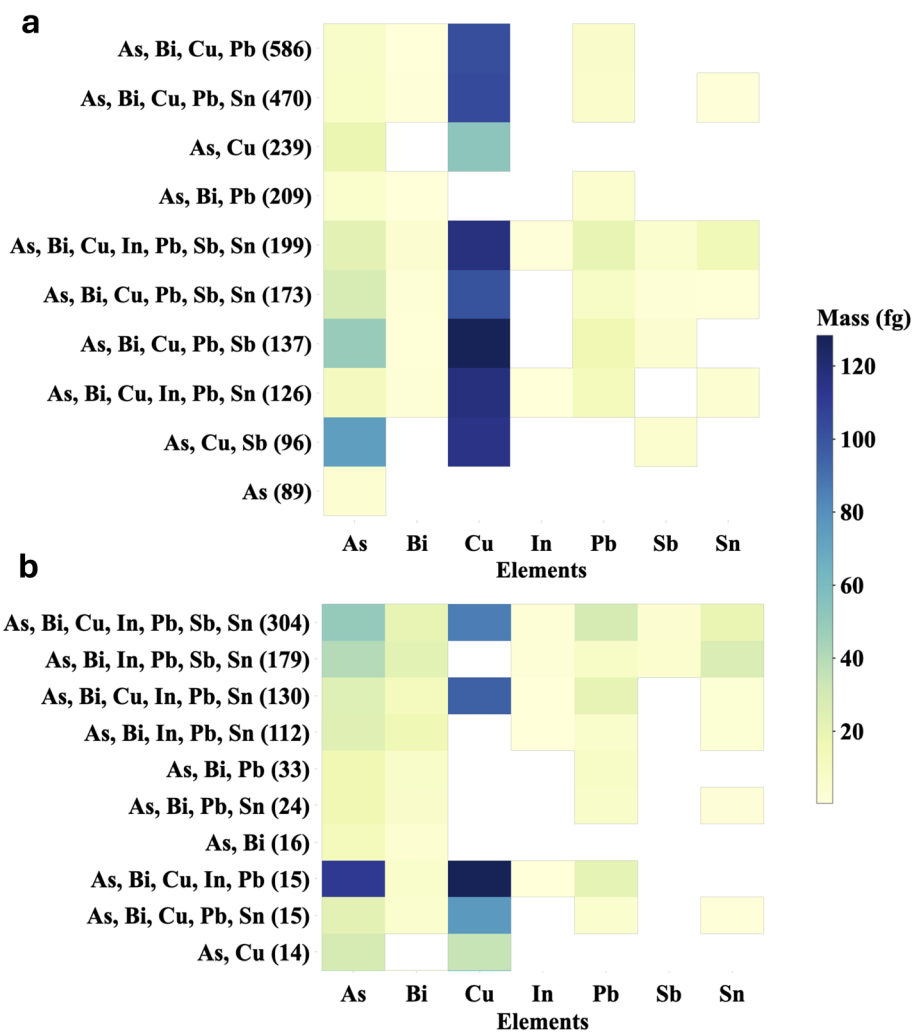

Fig. 5 Heatmaps displaying the multi-element composition of the 10 most frequent As-bearing particle combinations at the truck wash (a) and reactor vent (b) locations. The numbers in parentheses indicate the number of individual particles detected for each elemental combination (total of 6951 As-containing particles were detected in (a); 945 particles were detected in (b). Note that many additional elements (*e.g.* Fe, Al, Si) are not included in this heatmap, although they were present in many particles. Up to 21 elements were detected in individual As particles.

In in most of the RV particles, whereas it is absent in most of the TW particles. Moreover, Cu is present in a far greater number of TW particles compared to RV. These differences support our fingerprinting strategy and our hypothesis that chemically distinct forms of As are emitted from the smelting process and feedstock handling. The high throughput capability of spICP-ToF-MS is also demonstrated; Fig. 5a shows the composition of 2324 of the 6951 characterized As particles, while 5b shows 842 of 945 total As particles.

When using multi-element signatures acquired by spICP-ToF-MS to identify particle types, detection limits must be considered. Minor or trace particle constituents may be undetected, especially those elements with poor sensitivity. This is most problematic in the smallest particles (those with lowest total mass). The main differences between Fig. 5a and b involve the presence or absence of Cu and In. When Cu is present, it is generally abundant (indicated by darker colors on the heatmap), suggesting its absence is not due to it being a trace component of particles. Regarding the differing sensitivity of the elements, As has the lowest sensitivity of those considered. Since we focus on As-bearing particles, it is not likely that co-occurring trace elements are missed simply due to their detection limits. Finally, In could be systematically missed if it were present in trace quantities, especially in small As-bearing particles (with lower total mass). However, there was no significant difference in particle mass between particles with and without detectable In (Fig. S6). Thus, despite the limitations of the technique, the multi-element particle signatures appear to primarily reflect real differences in particle chemistry between the end-member environments.

Table 2 Particle classification scheme based on multi-element signature from spICP-TOFMS data

Particle class	Multi-element signature
Smelter	As; In (can include additional elements)
Ore mineral	As; Cu; Bi and/or Sb (without In)
Unknown	As only, As; Cu

The time-resolved classification results for As-bearing particles are presented in Fig. 6 for sample sets RL (6a), RV (6b), TW (6c), and LS (6d); results are plotted as the mass fraction of As attributed to each source; those derived from smelting, containing In and As, and As-bearing ore mineral particles, containing As, Cu, either Bi or Sb, and no In. Particle classification scheme is listed in Table 2.

Initially, on the loading side of the reactor building, nearly all As-bearing particles measured could be attributed to the smelting process, until an abrupt transition occurred within 8 minutes to bring the assignment of smelting derived particles to around 50%, with a corresponding increase in ore mineral particle signatures (Table S6). This transition corresponded within minutes to the time when concentrate began to be loaded into the storage bins in the reactor building, as indicated by the shaded box in Fig. 6a and b (Prevost, personal communication). On the vent side of the reactor, nearly all of the submicron particulate As could be attributed to the smelting process, with almost no contribution from ore minerals. Only a slight increase in ore mineral signatures was observed during the concentrate loading phase. These results strongly support

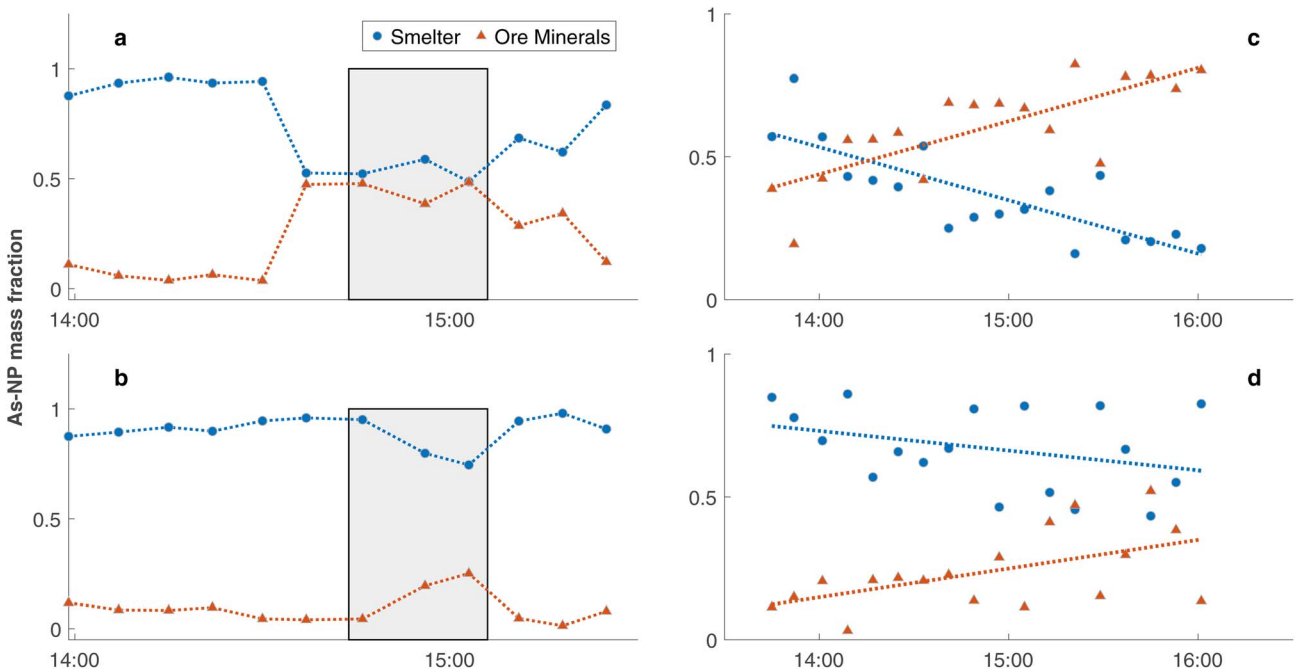

Fig. 6 Mass fraction of As-bearing sub-micron particles attributed to smelting-derived phases (blue) and ore mineral particles (orange) plotted as a function of time: (a) reactor building, loading section and (b) reactor building, venting section. (a) and (b) represent simultaneously collected sample sets, as do (c) truck wash station and (d) legal monitoring station. The grey rectangle in ((a) and (b)) represents the time during which the copper concentrate was loaded into storage bins inside the reactor building.

our trace element classification scheme, and further support that most of the As particles measured in the reactor building were created during the smelting process. The ability for this strategy, which was designed *a priori*, to reflect changing conditions inside the smelter was very encouraging.

Outside the smelter, particle signatures reflected changes in the emission source of the As particles with time, as a result of variable environmental conditions. At both the truck wash (Fig. 6c) and the legal station (Fig. 6d), the fraction of As from the ore mineral particles increased over time, at the expense of smelter-derived particles. However, ore mineral particles were more frequently observed at the truck wash, and increased more strongly compared to the legal station, where smelter-derived particles accounted for over half of most samples. The increase in ore mineral particle signatures at both sites is likely related to the road conditions within the smelter complex. Rain fell for several hours prior to sampling and stopped roughly 30 minutes before the sampling period began. Subsequently, temperatures rose and clouds dissipated, resulting in the road drying over the ~3 hours sampling period. The dry road conditions allowed for suspension of more mineral particles as concentrate-hauling trucks drove past the sampling location, whereas particles were likely less mobile when the road was wet. The As particle classification at the legal station was consistent with previous results showing that some As likely originated from dust emissions, although a greater fraction was from the smelter. These results support limited off-site transport of the feedstock particles compared to direct emissions from smelting.

It is noteworthy that the single particle data clearly showed time-resolved trends in As emission sources (Fig. 6), while the bulk-scale approaches (Fig. 4) were only able to compare combined sample sets. Using the bulk-scale approaches (water soluble fraction, Cu : As ratio), only a single value was obtained per time point. Such values are subject to uncertainty, most notably the "nugget effect" where one large particle could dominate the bulk signature obtained.[34] This necessitates grouping of the entire sample set, and thus more limited interpretations. By contrast, each point in Fig. 6 represented the compositions of many As-bearing particles (24–1272 per sample), providing more robust statistics and thus much clearer trends with time.

Finally, in order to validate the hypothesis that As-bearing particles associated with feedstock transport are chemically and mineralogically distinct from those emitted during the smelting process, two samples were analyzed by automated mineralogy (AM) and SEM-EDS: an air filter sample collected on a roof 0.5 km from the smelter complex and a dust sample collected from the road along which feedstock is transported. Many As-bearing particles were detected in each sample, including arsenates, native As, As oxides, and Cu–As sulfides. In the road dust sample, the As was overwhelmingly found within Cu–As sulfide minerals, accounting for 89% of the As-containing pixels mapped by AM (Table S7). Furthermore, the vast majority of the 11% of pixels not contained in the sulfides were found within a single large (400 μm) particle of As (Fig. 7D and E). In contrast, 97% of the As-containing pixels found on the filter of airborne particulates were classified as arsenates, arsenic oxides, or native arsenic, with only 3% being associated with sulfides (Table S7). SEM backscatter images of several As-bearing particle types are presented in Fig. 7.

Three As-bearing phases detected on the filter sample are presented in Fig. 7A–C, including an As–Pb–Cd oxide grain (Fig. 7A), an As-rich rim on an aluminosilicate grain (Fig. 7B),

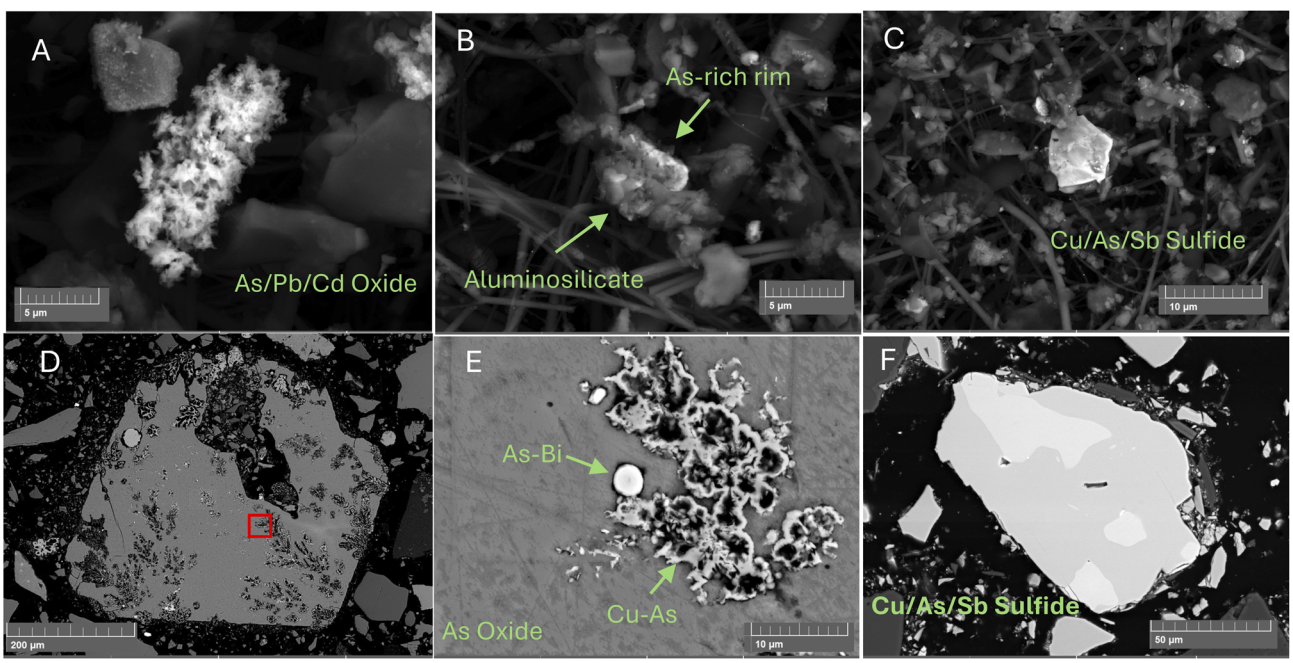

Fig. 7 Scanning electron microscope images of three As-bearing phases identified from an air filter sample (A–C), and in a sample of road dust from the smelter grounds (D–F). The red box in (D) indicates the section presented in (E).

and a Cu–As–Sb sulfide grain (Fig. 7C). These grains reflect the diversity of particulate phases transported by wind away from the smelter complex. The grain in Fig. 7A is very likely to have condensed from vapor originating from the smelting process, as indicated by its porous, honeycomb-like texture and elemental composition, consisting of volatile elements, but no Cu or S. The As-rich zone on the grain in Fig. 7B may have also condensed from vapor onto the aluminosilicate host grain. This could have occurred within the smelter, if the host grain was a flux or slag particle, or outside the smelter, if the host grain was an airborne mineral dust particle. The grain in Fig. 7C is likely an unreacted ore mineral particle, rich in Cu and S, indicating a copper sulfide, with significant As and minor Sb, possibly an enargite grain. Because the overwhelming majority of detected As particles on the filter were not sulfide minerals, the hypothesis that the majority of the airborne off-site As is of a smelting origin is supported.

The majority of the large grain in Fig. 7D was As (78% by EDS), with 15% oxygen (Fig. S7). The increased magnification in Fig. 7E shows complex textures and elemental compositions, including droplets of As–Bi and a corrosion texture infilled with Cu–As. This grain clearly originated from smelting, but is unlikely to have condensed from vapor. Rather, it is likely to have been crystalized from liquid form, perhaps in the slag phase. It is noteworthy that particles similar to the porous As–Pb–Cd oxide phases seen in the filter sample (Fig. 7A–C) were not observed in the road dust. Rather, the grain pictured in Fig. 7F represented the majority of As phases measured in this sample. It is a Cu–As-sulfide ore mineral with trace Sb, possibly enargite (Cu_3AsS_4), which likely originated from feedstock transport.

4 Conclusions

Using high temporal resolution sampling (8 minutes) of aerosols and a variety of chemical and mineralogical analyses, this study revealed several important characteristics of As emissions from the smelter. First, they are highly variable both within the smelter complex and in the surrounding area, with a nearly 10 000-fold difference in airborne As concentrations among the sample sets collected in this study. Moreover, at fixed locations, airborne As is highly variable on short (10–20 minutes) time scales. Understanding atmospheric emissions from point sources at high time resolution is critical for both precise source apportionment (*e.g.* specific processes within the smelter) and to better understand environmental and human health impacts (*e.g.* transient *vs.* continuous exposure). Using two sampling devices, we observed different distance-dependent relationships in simultaneous measurements of airborne As concentrations between two sample sets. Elevated As at a proximal site may indicate a ground level emission, while elevated As at a distal site may indicate an emission from the stack (although more work is needed to verify this). The identification of these point sources is essential for future efforts to curb emissions.

Bulk geochemical properties of airborne As, including the Cu : As ratio and the water-soluble fraction of As at two end-member environments, were used to contrast the two likely sources of As emission from the smelter site (As-bearing sulfide mineral particles at the truck wash and As phases condensed from vapor in the reactor building). The greatest difference between these environments was seen in the water-soluble fraction of As, results which shed new light on the high degree of solubility of the freshly condensed As-bearing particles from smelting.

Single particle techniques, especially spICP-ToF-MS, provided the greatest insights into the emission sources. Based upon the co-occurrence of trace elements including In, Bi, and Sb in the As-bearing particles, individual particles could be classified as originating from smelting, or from ore minerals. Using this approach, changes in the sampling environment through time were detected, including the transportation of concentrate within the reactor building and the drying of the road, which led to increased mobilization of mineral particles from trucking. While SEM-EDS and automated mineralogy of two complimentary samples identified particles that likely originated from the two hypothesized sources of As, analysis by spICP-ToF-MS offered two distinct advantages. First, although trace elements, including In, were critical to identifying the source(s) of the particles, In was not detected by EDS in any of the particles. Second, preparation and analysis of two samples by microscopy required roughly the same time as 155 samples by spICP-ToF-MS.

The fingerprinting strategies developed herein should be applied to larger sample sets in the future. Collection of additional samples during different environmental conditions, and during specific processes occurring within the smelter is likely to result in a better understanding of As emissions to the surrounding community.

Author contributions

A. G., K. W., and P. H. designed the experiments. A. G., E. N., and TG conducted the field sampling. A. G., H. E. A., T. G., and F. K. performed the analysis and data interpretation. A. G. prepared the manuscript with input from all co-authors.

Conflicts of interest

We declare no competing interests.

Data availability

All data used to generate figures is included in the supplementary information (SI), with the exception of the full results of the raw spICP-TOFMS data. These data will be published on Zenodo upon publication of the manuscript. Supplementary information is available. See DOI: https://doi.org/10.1039/d6ea00056h.

Acknowledgements

The authors acknowledge funding from Fonds de recherche du Québec – Nature et technologies (FRQNT), the Natural Sciences and Engineering Research Council (NSERC), EcotoQ, Canada

Foundation for Innovation and Glencore. We thank Daniel Proulx and the ONICSE organization for providing access to some of the sampling locations. We thank Glencore for providing site access, road dust samples and insights into the smelting process. We thank Mohamad Kanj, Marie-Pier Reid, and Arnold Downey for assistance with field sampling. We thank the Colorado School of Mines Center for Environmental Risk Assessment for the loan of one of the Coriolis samplers.

References

1 K. S. Mohammed Abdul, S. S. Jayasinghe, E. P. S. Chandana, C. Jayasumana and P. M. C. S. De Silva, Arsenic and Human Health Effects: A Review, *Environ. Toxicol. Pharmacol.*, 2015, 828–846, DOI: 10.1016/j.etap.2015.09.016.

2 W. H. Schlesinger, E. M. Klein and A. Vengosh, The Global Biogeochemical Cycle of Arsenic, *Global Biogeochemical Cycles*. John Wiley and Sons Inc November, vol. 1, 2022. DOI: 10.1029/2022GB007515.

3 R. Martin, K. Dowling, D. Pearce, J. Sillitoe and S. Florentine, Health Effects Associated with Inhalation of Airborne Arsenic Arising from Mining Operations, *Geosciences*, 2014, 128–175, DOI: 10.3390/geosciences4030128.

4 J. Podgorski and M. Berg, Global Threat of Arsenic in Groundwater. https://www.science.org.

5 M. A. Rahman and H. Hasegawa, High Levels of Inorganic Arsenic in Rice in Areas Where Arsenic-Contaminated Water Is Used for Irrigation and Cooking, *Sci. Total Environ.*, 2011, **15**, 4645–4655, DOI: 10.1016/j.scitotenv.2011.07.068.

6 M. M. Savard, G. F. Bonham-Carter and C. M. Banic, A Geoscientific Perspective on Airborne Smelter Emissions of Metals in the Environment: An Overview, *Geochem. Explor. Environ. Anal.*, 2006, (6), 99–109.

7 P. Brimblecombe, Atmospheric Arsenic, *Nature*, 1979, **280**, 5718.

8 K. H. Telmer, B. Daneshfar, M. S. Sanborn, D. Kliza-Petelle and D. G. Rancourt, *The Role of Smelter Emissions and Element Remobilization in the Sediment Chemistry of 99 Lakes Around the Horne Smelter, Québec*, 2006, Vol. 6.

9 H. K. T. Wong, C. M. Banic, S. Robert, Z. Nejedly and J. L. Campbell, In-Stack and in-Plume Characterization of Particulate Metals Emitted from a Copper Smelter, *Geochem. Explor. Environ. Anal.*, 2006, **6**(2–3), 131–137, DOI: 10.1144/1467-7873/05-083.

10 J. Dupont, D. E. Ponton, A. Marois, N. J. Fenton, M. Amyot and M. Rosabal, Elemental Atmospheric Deposition around North America's Largest Metal Processor of Electronic Waste (Horne Smelter, Canada), *Front. Environ. Chem.*, 2025, **6**, 1505053, DOI: 10.3389/fenvc.2025.1505053.

11 J. N. Caplette, M. Schindler and T. K. Kyser, The Black Rock Coatings in Rouyn-Noranda, Québec: Fingerprints of Historical Smelter Emissions and the Local Ore, *Can. J. Earth Sci.*, 2015, **52**(11), 952–965, DOI: 10.1139/cjes-2015-0064.

12 K. Telmer, G. F. Bonham-Carter, D. A. Kliza and G. E. M. Hall, The Atmospheric Transport and Deposition of Smelter Emissions: Evidence from the Multi-Element Geochemistry of Snow, Quebec, Canada, *Geochim. Cosmochim. Acta*, 2004, **68**(14), 2961–2980, DOI: 10.1016/j.gca.2003.12.022.

13 K. Delbeke, *Copper Concentrates: Environmental and Human Health Hazard Classification*, 2014.

14 X. Wan, D. Sukhomlinov, P. Taskinen, M. Lindgren, R. Michallik and A. Jokilaakso, Arsenic Condensation and Reaction Mechanisms in Flash Smelting Off-Gas Line Conditions, *Metall. Mater. Trans. B*, 2023, **54**(5), 2747–2757, DOI: 10.1007/s11663-023-02871-9.

15 I. J. Weisenberg, P. S. Bakshi, S. Monica and A. E. Vervaert, Arsenic Distribution and Control in Copper Smelters, *JOM*, 1979, **31**, 38–44.

16 A. Davis, M. Ruby, M. Bloom, R. Schoof, G. Freeman and P. Bergstrom, Mineralogic Constraints on the Bioavailability of Arsenic in Smelter-Impacted Soils, *Environ. Sci. Technol.*, 1996, **30**, 392–399.

17 Y. Tardif, L. Richard, D. Bellamy, H. E. Ahabchane, M. Tharaud, L. Schlatt, A. Dourlent, N. Trieu, J. King, K. J. Wilkinson and P. L. Hayes, Contrasting the Elemental Composition of Fine Particulate Matter in Urban and Remote Samples Using Single Particle Inductively Coupled Plasma Time-of-Flight Mass Spectrometry (SP ICP-ToF-MS), *Aerosol Sci. Technol.*, 2025, **59**(9), 1065–1081, DOI: 10.1080/02786826.2025.2519091.

18 A. J. Goodman, H.-E. Ahabchane, P. L. Hayes and K. J. Wilkinson, Characterizing Atmospheric Emissions of Particulate Matter from Copper Smelting through Coriolis-μ Air Sampling and Single Particle ICP–MS Analysis, *ACS ES&T Air*, 2026, **3**(2), 385–395, DOI: 10.1021/acsestair.5c00307.

19 A. Delater, M. Plumail, G. Uzu, L. Meunier, S. Fable, M. Floreani, C. Gamez, T. Mhadhbi, J. Queron, O. Le Bihan, I. Coll, B. Berthelot and G. Lacroix, Air Cyclone Samplers for Assessing the Toxicological Potential of Particulate Matter: A Case Study in Railway Environments, *Aerosol Sci. Technol.*, 2026, **60**(2), 168–184, DOI: 10.1080/02786826.2025.2568698.

20 N. R. de Sousa, L. Shen, D. Silcott, C. J. Call and A. G. Rothfuchs, Operative and Technical Modifications to the Coriolis® μ Air Sampler That Improve Sample Recovery and Biosafety during Microbiological Air Sampling, *Ann. Work Expo. Health*, 2020, **64**(8), 852–865, DOI: 10.1093/ANNWEH/WXAA053.

21 C. Wolk, *Invisible Damage, Imaginary Injuries, And The Political Ecology Of Redress In A Quebec Mining And Smelter Town*, 2023.

22 T. E. Lockwood, R. Gonzalez de Vega, Z. Du, L. Schlatt, X. Xu and D. Clases, Strategies to Enhance Figures of Merit in ICP-ToF-MS, *J. Anal. At. Spectrom.*, 2023, **39**(1), 227–234, DOI: 10.1039/d3ja00288h.

23 H. Pace, N. Rogers, C. Jarolimek, V. Coleman, C. Higgins and J. Ranville, Determining Transport Efficiency for the Purpose of Counting and Sizing Nanoparticles via Single Particle Inductively Coupled Plasma Mass Spectrometry, *Anal. Chem.*, 2011, **83**(24), 9361–9369, DOI: 10.1021/ac201952t.

24 H. Ahabchane, A. Goodman, M. Hadioui and K. Wilkinson, IsotopeTrack: A Fast and Flexible Applicaton for the Analysis of SP-ICP-TOF-MS Datasets, *Environ. Chem.*, 2026, **23**(2), EN25111.
25 L. Hendriks, A. Gundlach-Graham and D. Günther, Performance of Sp-ICP-TOFMS with Signal Distributions Fitted to a Compound Poisson Model, *J. Anal. At. Spectrom.*, 2019, **34**(9), 1900–1909, DOI: 10.1039/c9ja00186g.
26 M. Lomax-Vogt, L. M. Carter, J. Wielinski, S. Kutuzov, G. V. Lowry, R. Sullivan, P. Gabrielli and J. W. Olesik, Challenges in Measuring Nanoparticles and Microparticles by Single Particle ICP-QMS and ICP-TOFMS: Size-Dependent Transport Efficiency and Limited Linear Dynamic Range, *J. Anal. At. Spectrom.*, 2025, **40**(3), 848–859, DOI: 10.1039/d4ja00425f.
27 M. S. Germani, M. Small and W. H. Zoller, Fractionation of Elements during Copper Smelting, *Environ. Sci. Technol.*, 1981, **15**(3), 792.
28 A. Aracena, M. Véliz, O. Jerez, E. Balladares and M. Pérez-Tello, An Overview of the Behavior of Concentrates with Arsenic, Antimony, and Bismuth under Roasting Conditions, *Minerals*, 2023, **13**, 942, DOI: 10.3390/min13070942.
29 C. Banic, W. R. Leaitch, K. Strawbridge, R. Tanabe, H. Wong, C. Gariépy, A. Simonetti, Z. Nejedly, J. L. Campbell, J. Lu, J. Skeaff, D. Paktunc, J. I. MacPherson, S. Daggupaty, H. Geonac'h, A. Chatt and M. Lamoureux, The Physical and Chemical Evolution of Aerosols in Smelter and Power Plant Plumes: An Airborne Study, *Geochem. Explor. Environ. Anal.*, 2006, **6**(2–3), 111–120, DOI: 10.1144/1467-7873/05-098.
30 Y. Chen, Z. Zhao, P. Taskinen, Y. Liang, H. Ouyang, B. Peng, A. Jokilaakso, S. Zhou, T. Chen, N. Peng and H. Liu, Characterization of Copper Smelting Flue Dusts from a Bottom-Blowing Bath Smelting Furnace and a Flash Smelting Furnace, *Metall. Mater. Trans. B*, 2020, **51**(6), 2596–2608, DOI: 10.1007/s11663-020-01907-8.
31 T. T. Werner, G. M. Mudd and S. M. Jowitt, The World's by-Product and Critical Metal Resources Part III: A Global Assessment of Indium, *Ore Geol. Rev.*, 2017, **86**, 939–956, DOI: 10.1016/j.oregeorev.2017.01.015.
32 O. Mejías, A. Parbhakar-Fox, L. Jackson, R. Valenta and B. Townley, Indium in Ore Deposits and Mine Waste Environments: Geochemistry, Mineralogy, and Opportunities for Recovery, *J. Geochem. Explor.*, 2023, **255**, 107312, DOI: 10.1016/j.gexplo.2023.107312.
33 S. Zhang, Y. Ding, B. Liu and C. chi. Chang, Supply and Demand of Some Critical Metals and Present Status of Their Recycling in WEEE, *Waste Manage.*, 2017, 113–127, DOI: 10.1016/j.wasman.2017.04.003.
34 P. M. Gy, *Sampling of Particulate Materials Theory and Practice*, Elsevier, 1979.

